Lattice Boltzmann method for double-diffusive natural convection

F. Verhaeghe,* B. Blanpain, and P. Wollants
Department of Metallurgy and Materials Engineering, Katholieke Universiteit Leuven, Belgium
(Received 9 November 2006; published 12 April 2007)

A lattice Boltzmann method for double-diffusive natural convection is presented. The model combines a multicomponent lattice Boltzmann scheme with a finite-difference solution of the energy equation to simulate natural convection caused by gradients in temperature and concentration. The model is validated both in two and three dimensions, and the agreement with literature data is satisfactory. A case study of thermosolutal convection of air in a cubical enclosure with horizontal thermal and solutal gradients is presented, exhibiting a rich variety of flow structures.

DOI: 10.1103/PhysRevE.75.046705 PACS number(s): 47.11.−j, 02.70.Ns, 44.25.+f

I. INTRODUCTION

Double-diffusive or thermosolutal natural convection is usually defined as the flow behavior of a fluid subject to gradients of two or more scalar quantities with different diffusivities, causing fluid flow through buoyancy forces [1]. A wide variety of flow structures can be observed, depending on the orientation of the different gradients with respect to each other and with respect to gravity [2].

These phenomena are readily encountered in numerous areas, ranging from oceanography and geology over astrophysics to metallurgy. One important example is the solidification of a binary alloy, where the solute rejection gives rise to density differences in the liquid melt, which together with the temperature gradients in the system can give rise to double-diffusive convection phenomena.

Since the pioneering work by Turner [1,3,4], there has been a growing interest in this phenomenon, due to its importance in science and technology. Sezai and Mohamad [5] divide the studies on this topic broadly into two types. In the first type the concentration gradient is applied vertically, whereas the temperature gradient is applied horizontally, leading to a stably stratified flow. The second type of studies, which is of interest to the present study, applies both gradients in the horizontal direction. This problem has been studied from an experimental [6–10] and from an analytical or numerical [5,11–23] point of view.

From the nondimensionalization of the conservation equations of mass, momentum, energy, and concentration for a binary mixture of components A and B, five dimensionless numbers arise, namely the thermal Rayleigh number $\mathrm{Ra}_T = (|\boldsymbol{g}|\beta_T \Delta T L^3)/\nu\alpha$, the solutal Rayleigh number $\mathrm{Ra}_S = (|\boldsymbol{g}|\beta_S^A \Delta x_A L^3)/\nu\alpha$, the ratio of buoyancy forces $N = \beta_S \Delta x_A / \beta_T \Delta T$, the Prandtl number $\mathrm{Pr} = \nu/\alpha$, and the Lewis number $\mathrm{Le} = \alpha/D$. Some authors prefer to work with the thermal and solutal Grashof number, defined as $\mathrm{Gr}_T = \mathrm{Ra}_T/\mathrm{Pr}$ and $\mathrm{Gr}_S = \mathrm{Ra}_S/\mathrm{Sc}$, with $\mathrm{Sc} = \nu/D$ the Schmidt number. ΔT and Δx_A are typical temperature and concentration differences in the system, β_T and $\beta_S^A = -\beta_S^B$ are the thermal and solutal expansion coefficients, L is a characteristic length, $|\boldsymbol{g}|$ is the magnitude of the gravitational acceleration, and ν, α, and D are the viscosity, thermal diffusivity and diffusion coefficient. If the enclosure is not square or cubic, the aspect ratio A_z, and A_y in three dimensions, may play a role. Since only two components are present in the current work, all variables above can be defined for component A, with equivalent formulations in terms of B. The sign of N indicates whether the buoyancy forces due to temperature and concentration are cooperating ($N>0$) or opposing each other ($N<0$).

One of the first experimental studies on double-diffusive convection in enclosures has been presented by Kamotani *et al.* [6]. In this work flow structures in shallow enclosures are investigated in an electrochemical system containing a copper-sulfate acid solution, imposing fixed temperatures with heat exchangers and fixed concentrations at electrode surfaces through anodic and cathodic reactions. The authors started from steady state thermal convection flow fields, and found similar flow structures for augmenting and opposing buoyancy forces. For smaller buoyancy ratios, typically smaller than 6 (augmenting) or 10 (opposing), the flow is unicellular with secondary cells, whereas when the buoyancy ratio is larger, a three-layered flow structure emerges. It should however be noted that these experiments did not reach steady state, thereby limiting the applicability of the conclusions. Similar experiments have been performed by Jiang *et al.* [9] and Han and Kuehn [10]. Jiang *et al.* [9] studied the unsteady behavior at large Rayleigh numbers, observing three flow regimes, namely a multilayer flow regime, a secondary flow regime, and a mixed flow regime, the unsteady behavior being triggered by unsteady solutal boundary layers. Han and Kuehn [10] extended the parameter window and studied the development of double diffusive flow starting from the steady state pure thermal situation, for different aspect ratios of the enclosure. Lee *et al.* [7] used a water-salt system with vertical walls made of membranes in contact with supply reservoirs imposing constant temperature and concentrations, to study steady state flow structures. They found unicellular flow fields for high and low buoyancy ratios, and multilayer flow structures for intermediate values. Weaver and Viskanta [8] presented one of the few studies on thermosolutal convection in gases. Making use of condensation and evaporation to impose gas concentrations, the authors obtain flow structures for both augmenting and opposing buoyancy forces, and observe unsteady behavior under certain conditions. A summary of the dimensionless

*Electronic address: frederik.verhaeghe@mtm.kuleuven.be

TABLE I. Overview of the dimensionless parameters in previous experimental and numerical studies of double-diffusive natural convection (after [19]).

	Experimental work				
Authors	A_z	Pr	Le	Gr_T	N
Kamotani *et al.* [6]	0.13–0.55	7	300	$0-1.9\times10^6$	(±)4–40
Jiang *et al.* [9]	0.13–0.5	7	400–425	$5.7\times10^3-3.3\times10^6$	−102 to −2.8
Lee *et al.* [7]	0.2 and 2.0	4.0–7.9	60–197	$(\pm)2.43\times10^5-7.12\times10^7$	(±)2.7–72.3
Han and Kuehn [10]	1 and 4	7.8–8.8	261–333	$(\pm)1.4\times10^5-1.1\times10^6$	−24–13
	Numerical work in 2D				
Authors	A_z	Pr	Le	Gr_T	N
Han and Kuehn [13]	4	8	250	$-4\times10^5-3\times10^5$	−50–550
Béghein *et al.* [14]	1	0.71	0.5–5	1.41×10^7	−0.02 to −10
Hyun and Lee [24]	2	7	100	$1.97\times10^3-3.94\times10^7$	0.5–10000
Lee and Hyun [11]	2	7	100	$0.28\times10^6-1.97\times10^7$	−0.5 to −30
Bennacer and Gobin [17]	1	7	−1000	10^3-10^6	0.1–100
Gobin and Bennacer [18]	1–8	7	−1000	10^3-10^6	0.1–100
Bergman and Hyun [25]	1	0.02	7500	5×10^3	−0.1–10
Ghorayeb and Mojtabi [19]	1, 2, 4, and 7	1	2–151	$0<\mathrm{Gr}_T(\mathrm{Le}-1)<3\times10^4$	−1
Xin *et al.* [20]	1–4	1	1.2	10^4-10^5	−1
Ghorayeb *et al.* [22]	1	1	2–45	$4.75\times10^4-1.2\times10^5$	−1
	Numerical work in 3D				
Authors	A_z; A_y	Pr	Le	Gr_T	N
Sezai and Mohamad [5]	1	10	0.1–150	$10^4-2\times10^4$	−2–0
Bergeon and Knobloch [23]	1–6	1	11	0–4000	−1

quantities of these experimental studies can be found in Table I.

Several authors [16,19,20] performed a linear stability analysis of the purely diffusive solution, i.e., linear temperature and concentration gradients, in the case with equal and opposing buoyancy forces, i.e., $N=-1$, with Lewis numbers different from 1. Gobin and Bennacer [16] derived a linear stability criterium for the case of an infinite vertical fluid layer and find that the critical Rayleigh number solely depends on the Lewis number. Ghorayeb and Mojtabi [19] and Xin and co-workers [20] extended the analysis to confined rectangular cavities, investigating the influence of the aspect ratio of the cavity.

Numerical studies of thermosolutal convection are mainly two dimensional (2D). The dimensionless quantities of a number of studies can be found in Table I. Beyond the purely diffusive solution, most authors find at steady state either a unicellular structure, a unicellular structure with secondary cells in the corners, or a multilayered structure, depending on the parameters. Ghorayeb *et al.* [22] performed simulations beyond the steady state regime, showing oscillatory flow that can be either centro-symmetric or asymmetric single frequency flow.

Sezai and Mohamad [5] and Bergeon and Knobloch [23] show that in a substantial part of the cases, double-diffusive natural convection in enclosures is truly three dimensional (3D). Sezai and Mohamad [5] studied the effect of the thermal Rayleigh number, the Lewis number and the buoyancy ratio on the thermosolutal natural convection in a cubical enclosure subject to horizontal and opposing thermal and solutal gradients. Bergeon and Knobloch [23] undertook a linear and nonlinear study of double-diffusive flows with equal and opposing temperature and concentration gradients, studying the stability loss of the diffusive solution, the dynamical behavior close to this bifurcation point, and the effect of the aspect ratios.

In this paper we tackle the problem of double-diffusive natural convection with the lattice Boltzmann method (LBM). Over the last two decades, this mesoscopic modeling technique, with a sound basis in kinetic theory [26–29], has been successfully applied to problems such as flow in porous media [30–32], multicomponent [33–36], and multiphase [37–39] flows and particulate suspensions [40,41].

Various authors have also suggested models for thermal flows. Lallemand and Luo [42] classify these models into three categories, namely the passive scalar approach, in which the flow field and the temperature field are solved by two distinct sets of populations, with coupling from the flow field to the temperature field, methods including various shock capturing schemes to treat the fully compressible Eu-

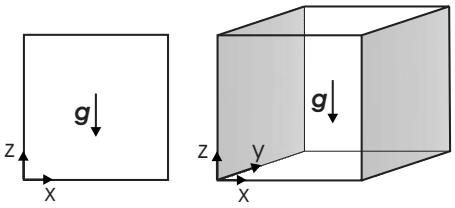

FIG. 1. Geometries used in the simulations. Left-hand side, 2D square, fixed temperature and concentration imposed on the left-hand and right-hand walls. Right-hand side, 3D cube, fixed temperature and concentration imposed on the grey faces. In both cases the gravity vector $\boldsymbol{g}$ points in the negative z direction.

ler or Navier-Stokes equations, and models extending athermal schemes with an energy conservation constraint. We refer to [42] for an in-depth discussion and references. Unfortunately the majority of the schemes suffer from numerical instability. The authors of [43] suggest a different approach, which is adopted in this work, namely to solve the temperature equation by a finite difference scheme, and to eliminate defects and numerical instability of previous schemes by adequate coupling between the lattice Boltzmann scheme for the flow field, and the finite difference scheme for the energy equation. A similar approach has been presented in [44]. We combine this approach with a lattice Boltzmann model for multicomponent liquids as presented by [35] with appropriate boundary conditions presented in [45].

The remainder of this paper is organized as follows. In Sec. II double-diffusive natural convection and the setup of the simulations is briefly introduced. Section III contains the description of the presented lattice Boltzmann model to describe this type of flow. The model is validated in Sec. IV. In Sec. V a numerical study of double-diffusive natural convection in a cubical enclosure is presented. Conclusions are formulated in Sec. VI.

II. PROBLEM STATEMENT

Double-diffusive phenomena arise because inhomogeneity of temperature and concentration give rise to density differences within the fluid. If these fluctuations can be assumed to be small, their effect can be modeled solely by a source term in the momentum conservation equation, a method known as the Boussinesq approximation [46]. In a binary fluid of components A and B, the density is described by a linear function of the temperature and the concentration x_A with respect to a reference density ρ_0 at a reference temperature T_0 and concentration x_A^0,

$$\rho = \rho_0[1 - \beta_T(T - T_0) - \beta_S^A(x_A - x_A^0)]. \tag{1}$$

Expression (1) is used in the body force,

$$\boldsymbol{F} = \boldsymbol{g}(\rho - \rho_0) \tag{2}$$

in which $\boldsymbol{g}$ is the gravitational acceleration.

The geometries used in this work are a square (2D) and cubical (3D) enclosure (see Fig. 1). At the walls, the macroscopic velocity of the binary mixture vanishes, i.e., $\boldsymbol{u}=0$ at the walls. The gravity vector points in the negative z direction. Constant but different temperatures, T_1 and T_2, and concentrations, $x_{A,1}$ and $x_{A,2}$ are imposed at the faces $x=0$ and $x=1$, whereas the other walls are assumed to be adiabatic, i.e., $\partial_n T=0$, and impermeable, i.e., $\partial_n x_A=0$.

It should be noted that the Boussinesq approximation linearizes the dependence of the density on the temperature and concentration, and the results can therefore only be expected to be valid for moderate temperature and concentration variations [47].

III. LATTICE BOLTZMANN MODEL FOR DOUBLE-DIFFUSIVE NATURAL CONVECTION

A. Multicomponent lattice Boltzmann model

Several models have been suggested to describe the multicomponent mixtures within the lattice Boltzmann framework, based on pseudopotential interactions [33,37], on heuristic free energies [38] or directly derived from kinetic theory models [35,36]. It should be noted that also the earlier models, although originally derived in an *ad hoc* fashion, can be connected to kinetic theory. In this work we adopt a model by Luo and Girimaji [48], derived from the continuous kinetic theory model of Sirovich [49]. In this model a binary mixture is described by a set of evolution equations for the species density distribution functions f_q^A and f_q^B,

$$f_q^A(\boldsymbol{r} + \boldsymbol{c}_q, t+1) = f_q^A(\boldsymbol{r}, t) + J_q^{AA} + J_q^{AB} + F_q^A, \tag{3}$$

$$f_q^B(\boldsymbol{r} + \boldsymbol{c}_q, t+1) = f_q^B(\boldsymbol{r}, t) + J_q^{BB} + J_q^{BA} + F_q^B, \tag{4}$$

in which the index q runs over all velocity vectors $\boldsymbol{c}_q$ of the chosen set. In two dimensions we adopt the D2Q9 set, in three dimensions the D3Q19 set. The terms J_q^{AA} and J_q^{BB} are the collision operators accounting for collisions between like particles, and J_q^{AB} and J_q^{BA} the collision operators describing cross collisions between unlike particles. The former type of collision operator is approximated with a single-relaxation time or Bhatnager-Gross-Krook (BGK) model, while the cross collisions are incorporated through a force-coupling approach. We refer to [35] for details.

The terms F_q^A and F_q^B are the forcing terms to incorporate the buoyancy effects. Since a separate evolution equation is solved for every species, the forcing term in Eq. (2) must be imposed for every species individually, ensuring that the total force equals the one given in Eq. (2). This is accomplished by the following set:

$$\boldsymbol{F}^A = \boldsymbol{g}(\rho_A - \rho_A^0), \tag{5}$$

$$\boldsymbol{F}^B = \boldsymbol{g}(\rho_B - \rho_B^0), \tag{6}$$

in which the species density is also assumed to be a linear function of temperature and concentration,

$$\rho_A = \rho_A^0[\beta_T^A(T - T^0) + \beta_S^A(x_A - x_A^0)], \tag{7}$$

$$\rho_B = \rho_B^0[\beta_T^B(T - T^0) + \beta_S^B(x_B - x_B^0)]. \tag{8}$$

In this work we choose $\beta_T^A = \beta_T^B = \beta_T$. The implementation of these terms will be discussed in Sec. III C.

The macroscopic conserved species quantities are calculated as the velocity moments of the distribution functions,

$$\rho_k = \sum_q f_q^k, \tag{9}$$

$$\rho_k \boldsymbol{u}_k = \sum_q f_q^k \boldsymbol{c}_q, \tag{10}$$

and the mixture quantities are obtained from the species quantities as follows:

$$\rho = \sum_k \rho_k, \tag{11}$$

$$\rho \boldsymbol{u} = \sum_k \rho_k \boldsymbol{u}_k. \tag{12}$$

By means of the Chapman-Enskog analysis it can be shown [35] that this model leads to the Navier-Stokes equations for the mixture velocity, and the classical diffusion-advection equations for the mass concentration, in which the transport coefficients can be related to the relaxation rates used in the collision operators.

B. Finite-difference energy equation

Following the approach suggested in [42], we solve the energy equation,

$$\partial_t T + \boldsymbol{u} \cdot \boldsymbol{\nabla} T = \kappa \Delta T \tag{13}$$

with a finite difference scheme,

$$T(\boldsymbol{r}, t+1) = T(\boldsymbol{r}, t) - \boldsymbol{u} \cdot \boldsymbol{\nabla}^* T + \kappa \Delta^* T. \tag{14}$$

The time integration is performed with a forward Euler scheme. The principles to derive the spatial finite difference stencils for hybrid thermal lattice Boltzmann models can be found in [42]. For the D2Q9 model, the following polynomials,

$$\varphi_0 = 1 \tag{15}$$

$$\varphi_1 = x, \quad \varphi_2 = y, \tag{16}$$

$$\varphi_3 = (x^2 - y^2), \quad \varphi_4 = xy, \quad \varphi_5 = (x^2 + y^2), \tag{17}$$

$$\varphi_6 = x(x^2 - y^2), \quad \varphi_7 = y(x^2 - y^2), \tag{18}$$

$$\varphi_8 = (x^2 - y^2)^2, \tag{19}$$

are used to expand the function $T(x,y)$ in two-dimensional space,

$$T(x,y) = \sum_q a_q \varphi_q(x,y). \tag{20}$$

For a point in the bulk, the coefficients a_i are determined by imposing

$$T(x_i,y_i) = \sum_q a_q \varphi_q(x_i,y_i). \tag{21}$$

with $(x_i,y_i)=(0,0)$, $(\pm 1,0)$, $(0,\pm 1)$, and $(\pm 1,\pm 1)$. The derivatives of $T(x,y)$ are obtained by taking the derivatives of Eq. (20).

For the D3Q19 model, a similar approach is followed using

$$\begin{gathered}
\varphi_0 = 1, \\
\varphi_1 = x, \quad \varphi_2 = y, \quad \varphi_3 = z, \\
\varphi_4 = x^2 + y^2 + z^2, \quad \varphi_5 = (x^2 + y^2 + z^2), \\
\varphi_6 = x(x^2 + y^2 + z^2), \quad \varphi_7 = y(x^2 + y^2 + z^2), \\
\varphi_8 = z(x^2 + y^2 + z^2), \\
\varphi_9 = 3x^2 - y^2 - z^2, \quad \varphi_{10} = y^2 - z^2, \\
\varphi_{11} = xy, \quad \varphi_{12} = yz, \quad \varphi_{13} = xz, \\
\varphi_{14} = (x^2 + y^2 + z^2)(3x^2 - y^2 - z^2), \\
\varphi_{15} = (x^2 + y^2 + z^2)(y^2 - z^2), \\
\varphi_{16} = x(y^2 - z^2), \quad \varphi_{17} = y(z^2 - x^2), \\
\varphi_{18} = z(x^2 - y^2),
\end{gathered} \tag{22}$$

and the collocations points are $(x_i,y_i,z_i)=(0,0,0)$, $(\pm 1,0,0)$, $(0,\pm 1,0)$, $(0,0,\pm 1)$, $(\pm 1,\pm 1,0)$, $(\pm 1,0,\pm 1)$, and $(0,\pm 1,\pm 1)$.

C. Implementation of force term

In the past, quite some discussion and confusion has arisen concerning the correct implementation of forcing terms in lattice Boltzmann simulations. Our simulations have shown that the approach presented in [50] leads to a correct agreement between LBM simulations and validation results. To satisfy the mass conservation equation up to second order in the Chapman-Enskog analysis, it is preferable to perform the forcing in two steps, adding one half of the forcing before the collision step, and the other half after, and to use the momentum with one half of the forcing added before collision as the measured field for output. This method can be summarized with the following scheme (adapted for BGK from [42]):

Step 1. Advection of f_q^k.
Step 2. Addition of first half of the forcing term.
Step 3. collision of f_q^k.
Step 4. Addition of second half of the forcing term.

The forcing is added in both steps through the classical formula:

$$f_q'^k = f_q^k + 3w_q \boldsymbol{c}_q \frac{\boldsymbol{F}^k}{2} \tag{23}$$

with $k=A$ or B and w_q the weight factor associated with velocity $\boldsymbol{c}_q$, f' and f the populations after and before the addition of the forcing, and $\boldsymbol{F}^k$ is the forcing term as defined in Eq. (6).

D. Boundary conditions

In the validation cases presented below, various boundary conditions need to be imposed, both for the lattice Boltzmann part and for the finite-difference temperature calculation.

The boundary conditions for the lattice Boltzmann model impose conditions on the flow field and the concentration field. To impose a fixed concentration and a zero mixture velocity at the wall, the following conditions can be used [45]:

$$f_{\bar{q}}^A(\boldsymbol{x}, t+1) = 2\bar{x}_A[\tilde{f}_q^A(\boldsymbol{x}, t) + \tilde{f}_q^B(\mathbf{x}, t)] - \tilde{f}_q^A(\boldsymbol{x}, t), \tag{24}$$

$$f_{\bar{q}}^B(\boldsymbol{x}, t+1) = 2\bar{x}_B[\tilde{f}_q^A(\boldsymbol{x}, t) + \tilde{f}_q^B(\boldsymbol{x}, t)] - \tilde{f}_q^B(\boldsymbol{x}, t), \tag{25}$$

in which $\tilde{f}_q^c$ are populations after collision, and $f_{\bar{q}}^A$ populations after streaming, with $\boldsymbol{c}_{\bar{q}} = -\boldsymbol{c}_q$, and $\bar{x}_A$ and $\bar{x}_B = 1 - \bar{x}_A$ are the imposed concentrations.

A second set of boundary conditions is a no-flux condition for the concentration and zero mixture velocity at the wall, which is accomplished by the typical bounce-back boundary conditions for every species,

$$f_{\bar{q}}^A(\boldsymbol{x}, t+1) = \tilde{f}_q^A(\boldsymbol{x}, t), \tag{26}$$

$$f_{\bar{q}}^B(\boldsymbol{x}, t+1) = \tilde{f}_q^B(\boldsymbol{x}, t). \tag{27}$$

Since the lattice Boltzmann model is used to simulate the fluid flow and the mass transfer, and the boundary conditions given above locate the boundary half a lattice spacing outside the calculation domain, the stencil for the temperature calculation of boundary points is no longer symmetrical. The collocation conditions of the missing nodes are replaced by the boundary conditions. Figure 2 explains this principle for a node in the two-dimensional case next to a corner. The circles with full line indicate fluid nodes, the circles in dashed line are missing neighbors. These are replaced by fictitious nodes on the boundary, where the boundary condition needs to be satisfied. Taking the example of an imposed temperature T_E on the right wall, and an adiabatic top wall, the following condition is imposed on the empty squares:

$$T(x_\square, y_\square) = T_E \tag{28}$$

while on the full squares, a zero gradient is imposed:

$$\partial_z T(x_\blacksquare, y_\blacksquare) = 0. \tag{29}$$

For nodes on the intersection of two boundaries, a choice must be made. Numerical tests show that the result does not depend on this choice. The details of the different types of boundary stencils used can be found in Appendix A for the 2D case and Appendix B for the 3D case.

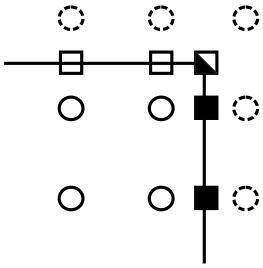

FIG. 2. Corner node at the intersection of two boundaries. Fluid nodes are indicated with full-line circles, missing nodes with dashed-line circles. Five neighboring nodes are not part of the computational domain. For the derivation of the stencil of the corner node, these are replaced by fictitious nodes on the boundary, indicated by the squares, where the boundary conditions are imposed. For nodes at the intersection of two boundaries, indicated here with a half-filled square, a choice must be made.

IV. VALIDATION

A. Case 1: Davis [51]

In his landmark paper, Davis [51] presented benchmark results for natural convection in a square cavity with differentially heated vertical side walls using a finite-difference code. Through mesh refinement and extrapolation accurate solutions are obtained for Rayleigh numbers from 10^3 to 10^6. To test our code, we performed simulations with the same Rayleigh numbers, both for pure thermally driven convection and for pure solutal natural convection.

Simulations are performed for Ra_T or Ra_S equal to 10^3, 10^4, 10^5, and 10^6, on a 200^2 grid for the first three Rayleigh numbers, and a 400^2 grid for the highest. If Ra_T is nonzero, Ra_S is zero and vice versa. The quantities calculated for comparison are presented in Table II. The local Nusselt number in the horizontal direction is calculated from

$$\mathrm{Nu}_{\mathrm{loc}}(x,z) = u(x,z)T(x,z) - \partial_x T(x,z). \tag{30}$$

For the calculation $\mathrm{Nu}_{\mathrm{loc}}$ in the bulk, a second order central difference approximation is used, whereas for boundary points, a first order one-sided finite difference approximation is used. For the calculation of the location of maxima and minima, the interpolation procedure from the initial work of Davis [51] is not used. Instead, the coordinate of the grid point where the maximum or minimum occurs is given.

In Table III the results obtained with the lattice Boltzmann model, both for pure thermal and pure solutal natural convection, are compared with the benchmark results of Davis [51]. The agreement is very good for all simulated Rayleigh numbers.

B. Case 2: Béghein *et al.* [14]

Béghein *et al.* [14] simulated double-diffusive natural convection in a square cavity.

Data is given for a fluid with $\mathrm{Le}=1$ for pure thermal convection with $\mathrm{Ra}_T = 2\times 10^4$, and for thermosolutal convection

TABLE II. Quantities used for comparison of the simulated results with the benchmark results of Davis [51].

u_{max}	Maximum horizontal velocity on the vertical midplane of the cavity
z_u	Location of the maximum horizontal velocity on the vertical midplane
v_{max}	Maximum vertical velocity on the horizontal midplane of the cavity
x_v	Location of the maximum vertical velocity on the horizontal midplane
$\bar{Nu}$	Average Nusselt number throughout the cavity
$Nu_{1/2}$	Average Nusselt number on the vertical midplane of the cavity
Nu_0	Average Nusselt number on the vertical boundary of the cavity at $x=0$
Nu_{max}	Maximum value of the local Nusselt number on the boundary at $x=0$
z_{max}	Location of maximum value of the local Nusselt number on the boundary at $x=0$
Nu_{min}	Minimum value of the local Nusselt number on the boundary at $x=0$
z_{min}	Location of minimum value of the local Nusselt number on the boundary at $x=0$

with $Ra_T=10^4$ and $Ra_S=10^4$, yielding the same result as for the pure thermal case, since thermal and solutal buoyancy augment each other. This data is compared with simulations using the present model on a 100^2 grid, for pure thermal convection [$Ra_T=2\times10^4$, thermal LBM (TLBM)], pure solutal convection [$Ra_S=2\times10^4$, multicomponent LBM (MCLBM)] and thermosolutal convection [$Ra_T=10^4$ and $Ra_S=10^4$, thermal multicomponent LBM (TMCLBM)], of which the results are shown, respectively, in Figs. 3–5. The

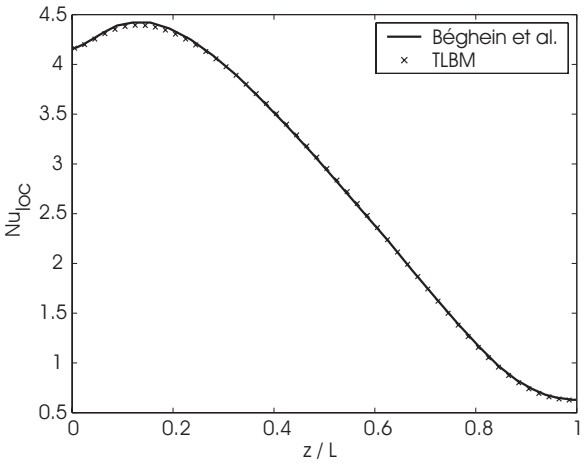

FIG. 3. Comparison of TLBM results with data from [14].

agreement is good in all three cases.

The authors also studied the effect of the buoyancy ratio N for opposing flows with Le=1. For a fixed thermal Rayleigh number $Ra_T=10^7$, the solutal Rayleigh number Ra_S is varied from 10^5 to 5×10^7, or equivalently, the buoyancy ratio N is varied from −0.01 to −5. Table IV shows the comparison of the results in Ref. [14] with the results obtained by the present method. The agreement is very good over the complete range of simulated buoyancy ratios.

C. Case 3: Fusegi *et al.* [52]

Fusegi and co-workers [52] performed simulations of three-dimensional thermally driven natural convection in a cubical enclosure. The working fluid is air, fixing Pr=0.71. The Rayleigh numbers range from $Ra_T=10^3$ to 10^6. The main purpose of the study by Fusegi *et al.* was to show the three-dimensional character of natural convection, in contrary to

TABLE III. Simulated results, both pure thermal (TLBM) and pure solutal (MCLBM), compared with the benchmark values of Davis [51], for Ra_T, respectively, Ra_S values of 10^3, 10^4, 10^5, and 10^6.

	Ra											
	10^3			10^4			10^5			10^6		
	Davis [51]	TLBM	MCLBM	Davis [51]	TLBM	MCLBM	Davis [51]	TLBM	MCLBM	Davis [51]	TLBM	MCLBM
u_{max}	3.649	3.649	3.649	16.178	16.180	16.181	34.73	34.70	34.72	64.63	64.65	64.77
z_u	0.813	0.813	0.813	0.823	0.823	0.823	0.855	0.853	0.853	0.850	0.853	0.858
w_{max}	3.697	3.697	3.697	19.617	19.621	19.622	68.59	68.53	68.57	219.36	219.14	219.73
x_w	0.178	0.178	0.178	0.119	0.118	0.118	0.066	0.068	0.068	0.0379	0.0375	0.0375
$\bar{Nu}$	1.118	1.118	1.118	2.243	2.244	2.244	4.519	4.516	4.517	8.800	8.774	8.782
$Nu_{1/2}$	1.118	1.118	1.118	2.243	2.244	2.244	4.519	4.514	4.515	8.799	8.768	8.886
Nu_0	1.117	1.118	1.118	2.238	2.244	2.244	4.509	4.520	4.521	8.817	8.809	8.816
Nu_{max}	1.505	1.506	1.506	3.528	3.530	3.531	7.717	7.713	7.713	17.925	17.440	17.447
z_{max}	0.092	0.088	0.088	0.143	0.143	0.143	0.081	0.083	0.083	0.0378	0.0375	0.0375
Nu_{min}	0.692	0.691	0.691	0.586	0.585	0.585	0.729	0.730	0.730	0.989	0.992	0.992
z_{min}	1	1	1	1	1	1	1	1	1	1	1	1

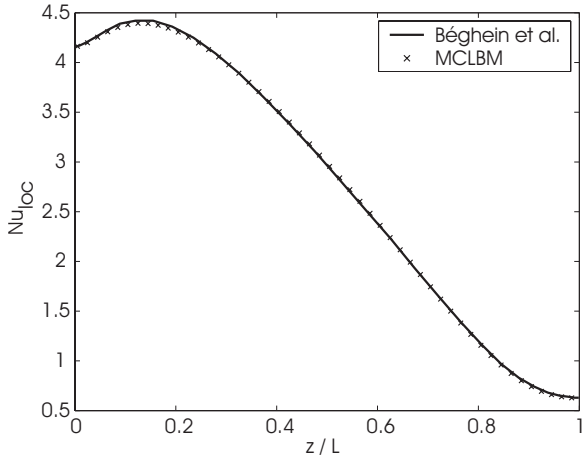

FIG. 4. Comparison of MCLBM results with data from [14].

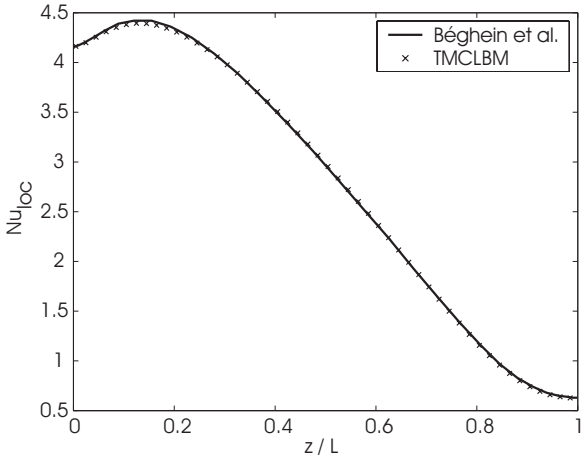

FIG. 5. Comparison of TMCLBM results with data from [14].

the usual two-dimensional assumption. We use their results as a benchmark for the model in this paper. We perform simulations of thermally driven convection with $Ra_T=10^3$, 10^4, 10^5, and 10^6 with $Ra_S=0$, and of concentration-driven convection $Ra_S=10^3$, 10^4, 10^5, and 10^6 with $Ra_T=0$. Table V shows the comparison of the LBM results with the results of Fusegi *et al.* for the mean Nusselt number at the isothermal walls.

The agreement is good, especially considering that in the case of the LBM simulations a uniform grid of 100^3 nodes is used, while Fusegi *et al.* [52] use a nonuniform grid to resolve the boundary layers. The use of nonuniform grids in LBM simulations is a logical extension of the current work and can be done similarly as in the work by Peng *et al.* [53].

V. RESULTS

In this section the results are presented of a numerical study which can be viewed as complementary to the one of Sezai and Mohamad [5]. The simulations in that article are for water based solutions (Pr=10), whereas in this work we focus on air (Pr=0.71) and investigate the role of the buoyancy ratio through a number of numerical experiments. We choose $Ra_T=10^5$ and Le=5 and study the flow structures for opposing driving forces with four buoyancy ratios, namely $N=-0.2$, $N=-0.5$, $N=-0.75$, and $N=-2$. For every case, the flow field, isotemperature and isoconcentration contours are presented in three planes, the mid-XZ plane, the XY plane at $z=0.9$, close to the top of the cavity, and the mid-YZ plane. The simulations are performed on a 100^3 grid.

For the lowest buoyancy ratio, i.e., $N=-0.2$, the results are shown in Fig. 6. The flow is mainly two dimensional: the isocontours of temperature and concentration in the XY and YZ planes are more or less parallel to the Y axis. The counter-clockwise flow field in the central XZ plane indicates that at this modest buoyancy ratio, the flow is mainly thermally driven. As can be expected for a Lewis number greater than 1, the solutal boundary layer is thinner than the thermal one, which can be clearly seen in the XZ plane. The center of the cavity is relatively homogeneous at a concentration of $x_A=0.5$.

The small three-dimensional effects which are already visible in the case of $N=-0.2$ are more pronounced at $N=-0.5$ in Fig. 7. The streamlines in the XY plane diverge towards the corners, and the four vortices appearing in the YZ plane are actually spiral structures. The distortion of the isocontours, especially of the concentration, indicate three-dimensional flow. At a buoyancy ratio of $N=-0.75$, closer to the case of equal but opposing forces, the three dimensionality is clear, and we find eight vortices in the YZ plane, clearly shown in Fig. 8. Now also the temperature contours become clearly distorted and the temperature field in the middle of the cavity becomes more homogeneous. In comparison to the results of Sezai and Mohamad, the three-dimensional character of the flow emerges only at values of N closer to unity, probably due to the lower Lewis number in the present simulations.

When the buoyancy ratio is increased to $N=-2$, a three-layered structure emerges, as can be seen in Fig. 9. Next to the thermally driven and hence counter-clockwise flowing central vortex, two solutally driven, clockwise rotating vortices emerge in the solutal boundary layer. The temperature and concentration contours tend to be more parallel to the Y

TABLE IV. Comparison of the lattice Boltzmann (LBM) results with the results of Beghein *et al.* (BG) for the average Sherwood number along a vertical axis for opposing flows with Le=1, Pr=0.71, and $Ra_T=10^7$. N is varied from −0.01 to −5.

Ra_S	10^5	10^6	2×10^6	5×10^6	8×10^6	9×10^6	1.5×10^7	5×10^7
N	−0.01	−0.1	−0.2	−0.5	−0.8	−0.9	−1.5	−5
Sh_{BG}	−16.4	−16.0	−15.5	−13.6	−10.6	−8.8	−13.6	−23.7
Sh_{LBM}	−16.4	−16.0	−15.5	−13.6	−10.6	−8.8	−13.7	−23.7

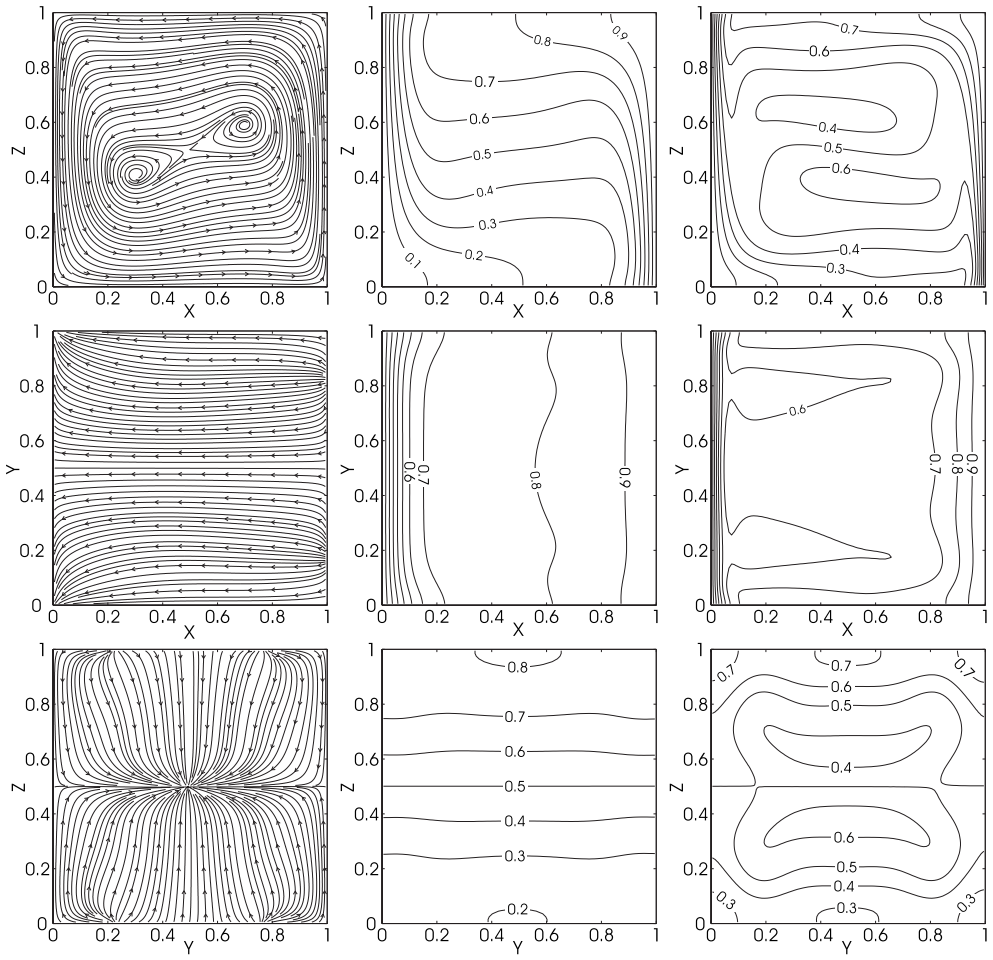

FIG. 6. Resulting fields for $N=-0.2$. Left-hand side, projected flow fields; center, isotemperature contours; right-hand side, isoconcentration contours. Top, plane $y=0.5$; middle, plane $z=0.9$; bottom, $x=0.5$.

axis, indicating a two-dimensional flow, yet four vortices persist in the *YZ* plane.

VI. CONCLUSIONS

In this paper we have presented a lattice Boltzmann method to study double-diffusive natural convection phenomena caused by temperature and concentration gradients in a multicomponent fluid in two and three dimensions. The model is validated against results obtained via other methods and the agreement is good in all cases, although it is also clear that further work can be done by extending the present method to nonuniform grids, to efficiently capture the boundary layers. The potentiality of the presented model is illustrated with a case study of the flow structure of thermosolutal convection of a binary gas in a cubical enclosure.

ACKNOWLEDGMENTS

One of the authors (F.V.) would like to acknowledge the support of the Research Foundation-Flanders (FWO-Vlaanderen) and would like to thank Prof. Li-Shi Luo, Prof. Pietro Asinari, and Dr. Yan Peng for the enlightening discussions.

TABLE V. Comparison of the average Nusselt or Sherwood number at the isothermal or isosolutal walls for the pure thermal LBM and the pure multicomponent model with the results of Fusegi *et al.* [52].

	Ra											
	10^3			10^4			10^5			10^6		
	Fusegi [52]	TLBM	MCLBM	Fusegi [52]	TLBM	MCLBM	Fusegi [52]	TLBM	MCLBM	Fusegi [52]	TLBM	MCLBM
Nu_{mean}	1.085	1.071	1.071	2.100	2.054	2.053	4.361	4.326	4.327	8.770	8.551	8.574

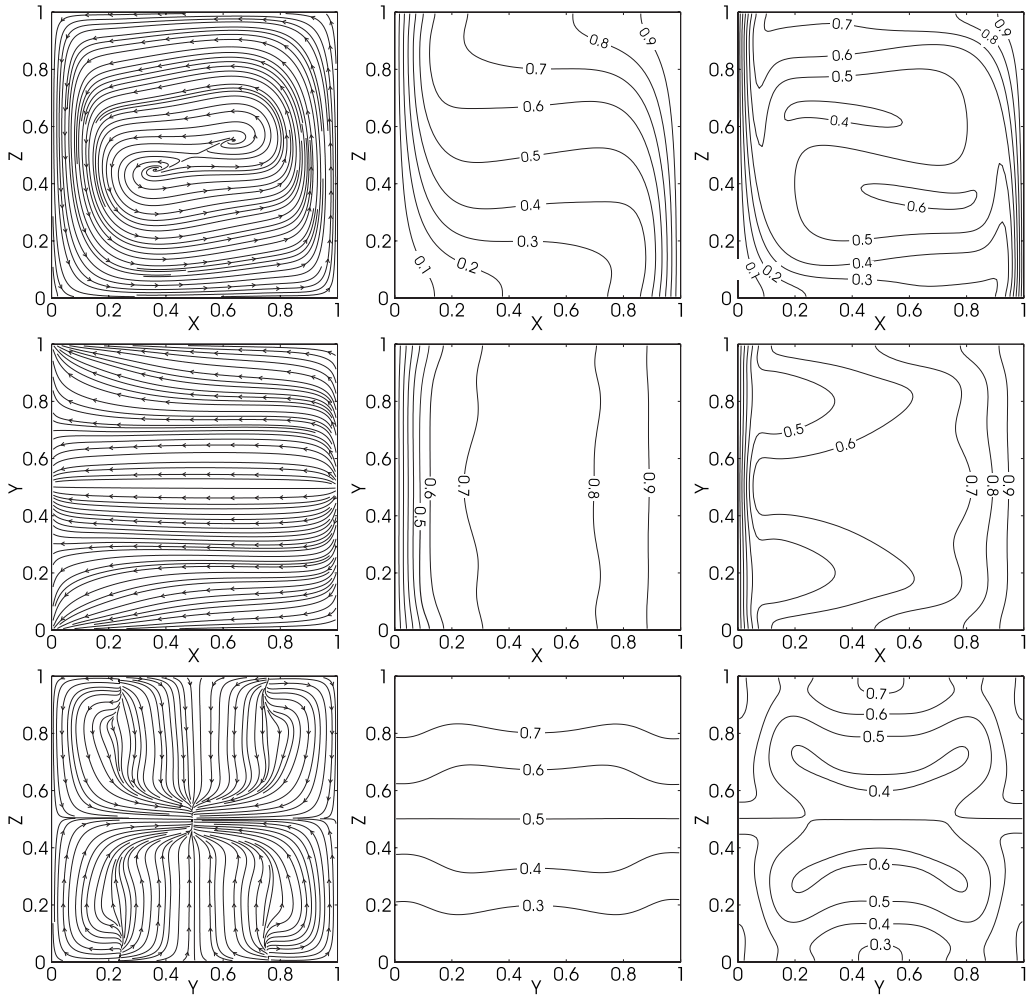

FIG. 7. Resulting fields for $N=-0.5$. Left-hand side, projected flow fields; center, isotemperature contours; right-hand side, isoconcentration contours. Top, plane $y=0.5$; middle, plane $z=0.9$; bottom, $x=0.5$.

APPENDIX A: FINITE DIFFERENCE STENCILS FOR TWO-DIMENSIONAL ENERGY EQUATION

In the two-dimensional simulations, the domain is discretized with n_x nodes in the x-direction, and n_z nodes in the z direction, so the domain consists of nodes (i,j) with $i=1,\ldots,n_x$ and $j=1,\ldots,n_z$. As was discussed supra, the number of fluid neighbors and the boundary conditions determine the stencil to be used for the temperature calculation. In what follows, the stencils are given explicitly for all possible cell types. The temperature imposed at $x=0$ is T_W, the one imposed at $x=1$ is T_E. The temperatures of neighboring cells are numbered in the same way as the velocity vectors, which is shown in Fig. 10. In this section and the next, the superscript of the operator has been dropped since it is clear that the operators given here are finite-difference operators.

1. Bulk cell

We have

$$\partial_x T = T_1 - T_3 - \frac{1}{4}(T_5 - T_6 + T_8 - T_7), \tag{A1}$$

$$\partial_y T = T_2 - T_4 - \frac{1}{4}(T_5 - T_8 + T_6 - T_7), \tag{A2}$$

$$\Delta T = 2(T_1 + T_2 + T_3 + T_4) - \frac{1}{2}(T_5 + T_6 + T_7 + T_8) - 6T_0. \tag{A3}$$

2. Faces

a. $i=n_x$

We have

$$\partial_x T = \frac{4}{3}T_E - \frac{5}{4}T_0 - \frac{7}{12}T_3 + \frac{1}{8}(T_2 + T_4 + T_6 + T_7),$$

$$\partial_y T = \frac{3}{2}(T_2 - T_4) - \frac{1}{3}(T_6 - T_7),$$

$$\Delta T = \frac{8}{3}T_E - \frac{17}{2}T_0 + \frac{9}{4}(T_2 + T_4) + \frac{17}{6}T_3 - \frac{3}{4}(T_6 + T_7).$$

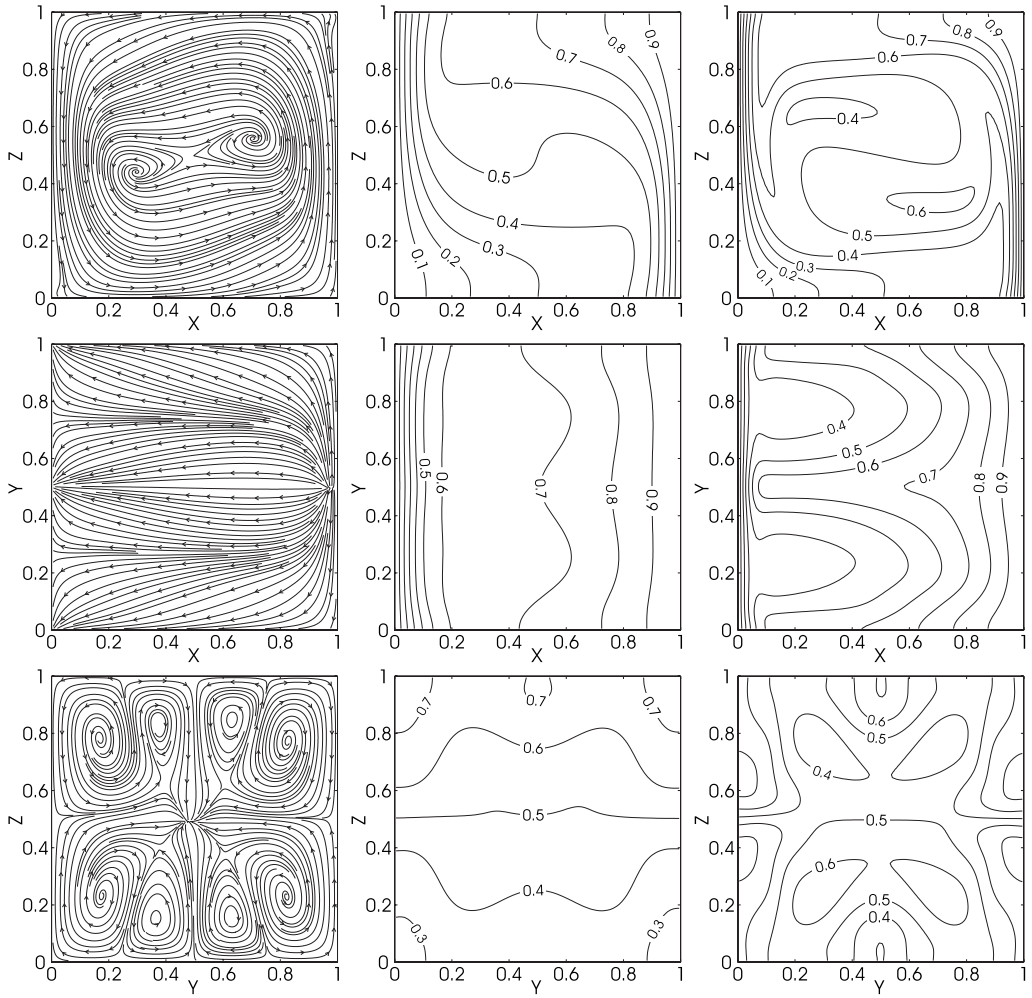

FIG. 8. Resulting fields for $N=-0.75$. Left-hand side, projected flow fields; center, isotemperature contours; right-hand side, isoconcentration contours. Top, plane $y=0.5$; middle, plane $z=0.9$; bottom, $x=0.5$.

b. i=1

We have

$$\partial_x T = -\frac{4}{3}T_W + \frac{5}{4}T_0 + \frac{7}{12}T_1 - \frac{1}{8}(T_1 + T_4 + T_5 + T_8),$$

$$\partial_y T = \frac{3}{2}(T_2 - T_4) - \frac{1}{3}(T_5 - T_8).$$

$$\Delta T = -\frac{8}{3}T_W - \frac{17}{2}T_0 + \frac{9}{4}(T_2 + T_4) + \frac{17}{6}T_1 - \frac{3}{4}(T_5 + T_8).$$

c. j=n_z

We have

$$\partial_x T = \frac{3}{4}(T_1 - T_3) - \frac{1}{4}(T_8 - T_7),$$

$$\partial_y T = T_0 - T_4 - \frac{1}{4}(T_1 + T_3) + \frac{1}{4}(T_7 + T_8),$$

$$\Delta T = -4T_0 + \frac{3}{2}(T_1 + T_3) + 2T_4 - \frac{1}{2}(T_7 + T_8).$$

d. j=1

We have

$$\partial_x T = \frac{3}{4}(T_1 - T_3) - \frac{1}{4}(T_5 - T_6),$$

$$\partial_y T = -T_0 + T_2 + \frac{1}{4}(T_1 + T_3) - \frac{1}{4}(T_5 + T_6),$$

$$\Delta T = -4T_0 + \frac{3}{2}(T_1 + T_3) + 2T_2 - \frac{1}{2}(T_5 + T_6).$$

3. Corners

a. i=n_x, j=n_z

We have

$$\partial_x T = \frac{4}{3}T_E - \frac{3}{4}T_0 - \frac{7}{12}T_3 - \frac{1}{4}T_4 + \frac{1}{4}T_7,$$

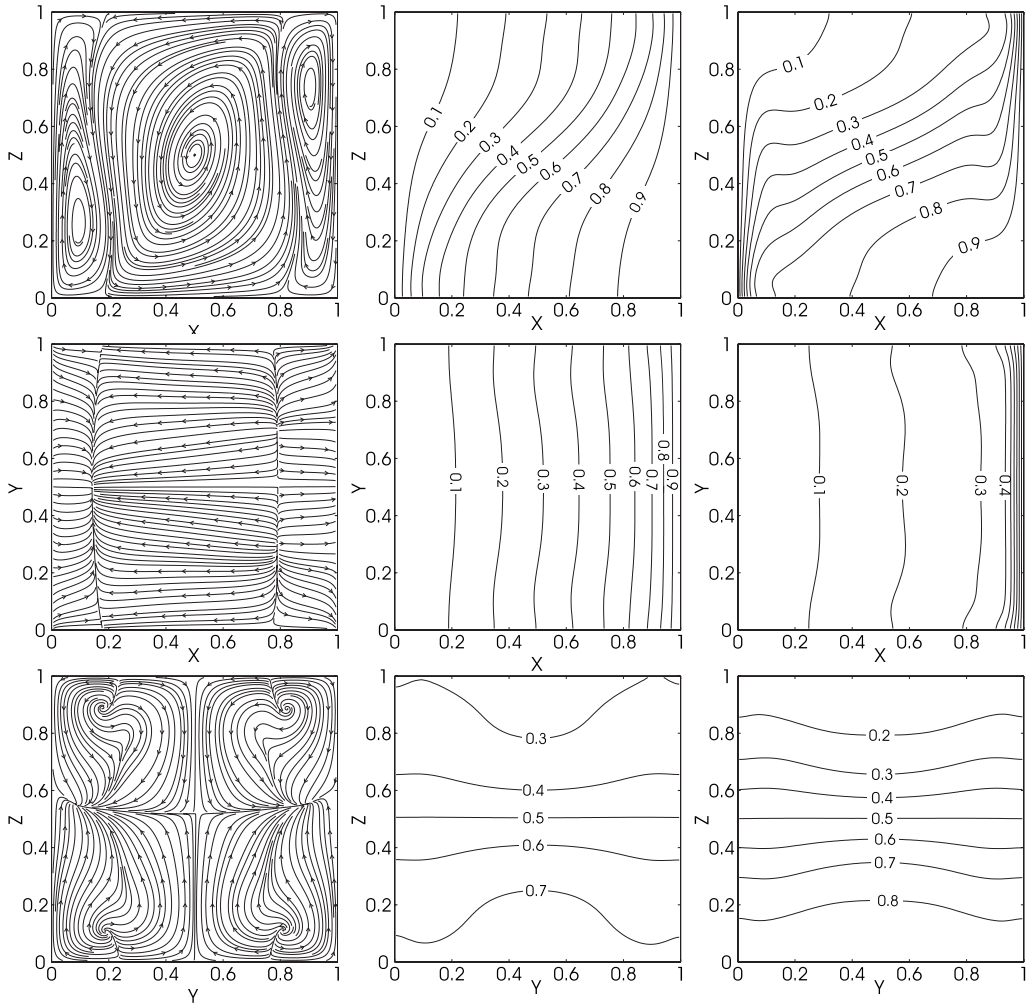

FIG. 9. Resulting fields for $N=-2$. Left-hand side, projected flow fields; center, isotemperature contours; right-hand side, isoconcentration contours. Top, plane $y=0.5$; middle, plane $z=0.9$; bottom, $x=0.5$.

$$\partial_y T = \frac{9}{4}(T_0 - T_4) - \frac{7}{12}(T_3 - T_7),$$

$$\Delta T = \frac{8}{3}T_E - 6T_0 + 2(T_3 + T_4) - \frac{2}{3}T_7.$$

b. $i=1$, $j=n_z$

We have

$$\partial_x T = -\frac{4}{3}T_W + \frac{3}{4}T_0 + \frac{7}{12}T_1 + \frac{1}{4}T_4 - \frac{1}{4}T_8,$$

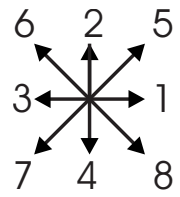

FIG. 10. Labeling of velocities and temperatures of neighbors for D2Q9 model.

$$\partial_y T = \frac{9}{4}(T_0 - T_4) - \frac{7}{12}(T_1 - T_8),$$

$$\Delta T = \frac{8}{3}T_W - 6T_0 + 2(T_1 + T_4) - \frac{2}{3}T_8.$$

c. $i=n_x$, $j=1$

We have

$$\partial_x T = \frac{4}{3}T_E - \frac{3}{4}T_0 - \frac{7}{12}T_3 - \frac{1}{4}T_2 + \frac{1}{4}T_6,$$

$$\partial_y T = \frac{9}{4}(T_2 - T_0) - \frac{7}{12}(T_3 - T_6),$$

$$\Delta T = \frac{8}{3}T_E - 6T_0 + 2(T_2 + T_3) - \frac{2}{3}T_6.$$

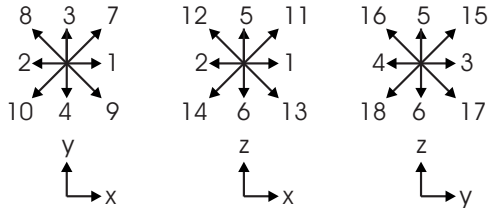

FIG. 11. Labeling of velocities and temperatures of neighbors for D3Q19 model.

d. i=1, j=1

We have

$$\partial_x T = -\frac{4}{3}T_W + \frac{3}{4}T_0 + \frac{7}{12}T_1 + \frac{1}{4}T_2 - \frac{1}{4}T_5,$$

$$\partial_y T = \frac{9}{4}(T_2 - T_0) - \frac{7}{12}(T_5 - T_1),$$

$$\Delta T = \frac{8}{3}T_W - 6T_0 + 2(T_1 + T_2) - \frac{2}{3}T_5.$$

APPENDIX B: FINITE DIFFERENCE STENCILS FOR THREE-DIMENSIONAL ENERGY EQUATION

In the three-dimensional simulations, the domain is discretized with n_x nodes in the x direction, n_y nodes in the y direction, and n_z nodes in the z direction, so the domain consists of nodes (i,j,k) with $i=1,\ldots,n_x$, $j=1,\ldots,n_y$, and $k=1,\ldots,n_z$. As was discussed supra, the number of fluid neighbors and the boundary conditions determine the stencil to be used for the temperature calculation. In what follows, the stencils are given explicitly for all possible cell types. The temperature imposed at $x=0$ is T_W, the one imposed at $x=1$ is T_E. The temperatures of neighboring cells are numbered in the same way as the velocity vectors, which is shown in Fig. 11.

1. Bulk cell

We have

$$\partial_x T = T_1 - T_2 - \frac{1}{8}(T_7 - T_8 + T_9 - T_{10} + T_{11} - T_{12} + T_{13} - T_{14}),$$

$$\partial_y T = T_3 - T_4 - \frac{1}{8}(T_7 + T_8 - T_9 - T_{10} + T_{15} - T_{16} + T_{17} - T_{18}),$$

$$\partial_z T = T_5 - T_6 - \frac{1}{8}(T_{11} + T_{12} - T_{13} - T_{14} + T_{15} + T_{16} - T_{17} - T_{18}),$$

$$\Delta T = -9T_0 + 2(T_1 + T_2 + T_3 + T_4 + T_5 + T_6) - \frac{1}{4}(T_7 + T_8 + T_9 + T_{10} + T_{11} + T_{12} + T_{13} + T_{14} + T_{15} + T_{16} + T_{17} + T_{18}).$$

2. Faces

a. i=n_x

We have

$$\partial_x T = \frac{4}{3}T_N - \frac{9}{8}T_0 - \frac{2}{3}T_2 + \frac{1}{16}(T_3 + T_4 + T_5 + T_6) + \frac{1}{12}(T_8 + T_{10} + T_{12} + T_{14}) - \frac{1}{32}(T_{15} + T_{16} + T_{17} + T_{18}),$$

$$\partial_y T = \frac{5}{4}(T_3 - T_4) - \frac{1}{6}(T_8 - T_{10}) - \frac{1}{8}(T_{15} - T_{16} + T_{17} - T_{18}),$$

$$\partial_z T = \frac{5}{4}(T_5 - T_6) - \frac{1}{6}(T_{12} - T_{14}) - \frac{1}{8}(T_{15} + T_{16} - T_{17} - T_{18}),$$

$$\Delta T = \frac{8}{3}T_N - \frac{45}{4}T_0 + \frac{8}{3}T_2 + \frac{17}{8}(T_3 + T_4 + T_5 + T_6) - \frac{1}{3}(T_8 + T_{10} + T_{12} + T_{14}) - \frac{5}{16}(T_{15} + T_{16} + T_{17} + T_{18}).$$

b. i=1

We have

$$\partial_x T = -\frac{4}{3}T_S + \frac{9}{8}T_0 + \frac{2}{3}T_1 - \frac{1}{16}(T_3 + T_4 + T_5 + T_6) - \frac{1}{12}(T_7 + T_9 + T_{11} + T_{13}) + \frac{1}{32}(T_{15} + T_{16} + T_{17} + T_{18}),$$

$$\partial_y T = \frac{5}{4}(T_3 - T_4) - \frac{1}{6}(T_7 - T_9) - \frac{1}{8}(T_{15} - T_{16} + T_{17} - T_{18}),$$

$$\partial_z T = \frac{5}{4}(T_5 - T_6) - \frac{1}{6}(T_{11} - T_{13}) - \frac{1}{8}(T_{15} + T_{16} - T_{17} - T_{18}),$$

$$\Delta T = \frac{8}{3}T_S - \frac{45}{4}T_0 + \frac{8}{3}T_1 + \frac{17}{8}(T_3 + T_4 + T_5 + T_6) - \frac{1}{3}(T_7 + T_9 + T_{11} + T_{13}) - \frac{5}{16}(T_{15} + T_{16} + T_{17} + T_{18}).$$

c. j=n_y

We have

$$\partial_x T = \frac{7}{8}(T_1 - T_2) - \frac{1}{8}(T_9 - T_{10} + T_{11} - T_{12} + T_{13} - T_{14}),$$

$$\partial_y T = \frac{15}{16}T_0 - \frac{5}{64}(T_1 + T_2 + T_5 + T_6) - \frac{17}{16}T_4 + \frac{9}{64}(T_9 + T_{10} + T_{16} + T_{18}) - \frac{1}{32}(T_{11} + T_{12} + T_{13} + T_{14}),$$

$$\partial_z T = \frac{7}{8}(T_5 - T_6) - \frac{1}{8}(T_{11} + T_{12} - T_{13} - T_{14} + T_{16} - T_{18}),$$

$$\Delta T = -\frac{57}{8}T_0 + \frac{59}{32}(T_1 + T_2 + T_5 + T_6) + \frac{15}{8}T_4 - \frac{7}{32}(T_9 + T_{10} + T_{16} + T_{18}) - \frac{5}{16}(T_{11} + T_{12} + T_{13} + T_{14}).$$

d. i=1

We have

$$\partial_x T = \frac{7}{8}(T_1 - T_2) - \frac{1}{8}(T_7 - T_8 + T_{11} - T_{12} + T_{13} - T_{14}),$$

$$\partial_y T = -\frac{15}{16}T_0 + \frac{5}{64}(T_1 + T_2 + T_5 + T_6) + \frac{17}{16}T_3 - \frac{9}{64}(T_7 + T_8 + T_{15} + T_{17}) + \frac{1}{32}(T_{11} + T_{12} + T_{13} + T_{14}),$$

$$\partial_z T = \frac{7}{8}(T_5 - T_6) - \frac{1}{8}(T_{11} + T_{12} - T_{13} - T_{14} + T_{15} - T_{17}),$$

$$\Delta T = -\frac{57}{8}T_0 + \frac{59}{32}(T_1 + T_2 + T_5 + T_6) + \frac{15}{8}T_3 - \frac{7}{32}(T_7 + T_8 + T_{15} + T_{17}) - \frac{5}{16}(T_{11} + T_{12} + T_{13} + T_{14}).$$

e. k=n_z

We have

$$\partial_x T = \frac{7}{8}(T_1 - T_2) - \frac{1}{8}(T_7 - T_8 + T_9 - T_{10} + T_{13} - T_{14}),$$

$$\partial_y T = \frac{7}{8}(T_3 - T_4) - \frac{1}{8}(T_7 + T_8 - T_9 - T_{10} + T_{17} - T_{18}),$$

$$\partial_z T = \frac{15}{16}T_0 - \frac{5}{64}(T_1 + T_2 + T_3 + T_4) - \frac{17}{16}T_6 + \frac{9}{64}(T_{13} + T_{14} + T_{17} + T_{18}) - \frac{1}{32}(T_7 + T_8 + T_9 + T_{10}),$$

$$\Delta T = -\frac{57}{8}T_0 + \frac{59}{32}(T_1 + T_2 + T_3 + T_4) + \frac{15}{8}T_6 - \frac{7}{32}(T_{13} + T_{14} + T_{17} + T_{18}) - \frac{5}{16}(T_7 + T_8 + T_9 + T_{10}).$$

f. k=1

We have

$$\partial_x T = \frac{7}{8}(T_1 - T_2) - \frac{1}{8}(T_7 - T_8 + T_9 - T_{10} + T_{11} - T_{12}),$$

$$\partial_y T = \frac{7}{8}(T_3 - T_4) - \frac{1}{8}(T_7 + T_8 - T_9 - T_{10} + T_{15} - T_{16}),$$

$$\partial_z T = -\frac{15}{16}T_0 + \frac{5}{64}(T_1 + T_2 + T_3 + T_4) + \frac{17}{16}T_5 - \frac{9}{64}(T_{11} + T_{12} + T_{15} + T_{16}) + \frac{1}{32}(T_7 + T_8 + T_9 + T_{10}),$$

$$\Delta T = -\frac{57}{8}T_0 + \frac{59}{32}(T_1 + T_2 + T_3 + T_4) + \frac{15}{8}T_5 - \frac{7}{32}(T_{11} + T_{12} + T_{15} + T_{16}) - \frac{5}{16}(T_7 + T_8 + T_9 + T_{10}).$$

3. Ribs

a. i=n_x, j=n_y

We have

$$\partial_x T = \frac{4}{3}T_N - T_0 - \frac{43}{72}T_2 + \frac{1}{48}(T_5 + T_6) + \frac{7}{72}T_{10} + \frac{1}{12}(T_{12} + T_{14}) - \frac{1}{48}(T_{16} + T_{18}),$$

$$\partial_y T = \frac{5}{4}T_0 - \frac{5}{36}T_2 - \frac{3}{2}T_4 - \frac{1}{24}(T_5 + T_6 + T_{12} + T_{14}) + \frac{2}{9}T_{10} + \frac{1}{6}(T_{16} + T_{18}),$$

$$\partial_z T = \frac{9}{8}(T_5 - T_6) - \frac{1}{6}(T_{12} - T_{14}) - \frac{1}{8}(T_{16} - T_{18}),$$

$$\Delta T = \frac{8}{3}T_N - \frac{19}{2}T_0 + \frac{89}{36}T_2 + 2T_4 + \frac{49}{24}(T_5 + T_6) - \frac{11}{36}T_{10} - \frac{5}{12}(T_{12} + T_{14}) - \frac{7}{24}(T_{16} + T_{18}).$$

b. i=n_x, j=1

We have

$$\partial_x T = \frac{4}{3}T_N - T_0 - \frac{43}{72}T_2 + \frac{1}{48}(T_5 + T_6) + \frac{7}{72}T_8 + \frac{1}{12}(T_{12} + T_{14}) - \frac{1}{48}(T_{15} + T_{17}),$$

$$\partial_y T = -\frac{5}{4}T_0 + \frac{5}{36}T_2 + \frac{3}{2}T_3 + \frac{1}{24}(T_5 + T_6 + T_{12} + T_{14}) - \frac{2}{9}T_8 - \frac{1}{6}(T_{15} + T_{17}),$$

$$\partial_z T = \frac{9}{8}(T_5 - T_6) - \frac{1}{6}(T_{12} - T_{14}) - \frac{1}{8}(T_{15} - T_{17}),$$

$$\Delta T = \frac{8}{3}T_N - \frac{19}{2}T_0 + \frac{89}{36}T_2 + 2T_3 + \frac{49}{24}(T_5 + T_6) - \frac{11}{36}T_8 - \frac{5}{12}(T_{12} + T_{14}) - \frac{7}{24}(T_{15} + T_{17}).$$

c. $i=n_x$, $k=n_z$

We have

$$\partial_x T = \frac{4}{3}T_N - T_0 - \frac{43}{72}T_2 + \frac{1}{48}(T_3 + T_4) + \frac{7}{72}T_{14} + \frac{1}{12}(T_8 + T_{10}) - \frac{1}{48}(T_{17} + T_{18}),$$

$$\partial_y T = \frac{9}{8}(T_3 - T_4) - \frac{1}{6}(T_8 - T_{10}) - \frac{1}{8}(T_{17} - T_{18}),$$

$$\partial_z T = \frac{5}{4}T_0 - \frac{5}{36}T_2 - \frac{3}{2}T_6 - \frac{1}{24}(T_3 + T_4 + T_8 + T_{10}) + \frac{2}{9}T_{14} + \frac{1}{6}(T_{17} + T_{18}),$$

$$\Delta T = \frac{8}{3}T_N - \frac{19}{2}T_0 + \frac{89}{36}T_2 + 2T_6 + \frac{49}{24}(T_3 + T_4) - \frac{11}{36}T_{14} - \frac{5}{12}(T_8 + T_{10}) - \frac{7}{24}(T_{17} + T_{18}).$$

d. $i=n_x$, $k=1$

We have

$$\partial_x T = \frac{4}{3}T_N - T_0 - \frac{43}{72}T_2 + \frac{1}{48}(T_3 + T_4) + \frac{7}{72}T_{12} + \frac{1}{12}(T_8 + T_{10}) - \frac{1}{48}(T_{15} + T_{16}),$$

$$\partial_y T = \frac{9}{8}(T_3 - T_4) - \frac{1}{6}(T_8 - T_{10}) - \frac{1}{8}(T_{15} - T_{16}),$$

$$\partial_z T = -\frac{5}{4}T_0 + \frac{5}{36}T_2 + \frac{3}{2}T_5 + \frac{1}{24}(T_3 + T_4 + T_8 + T_{10}) - \frac{2}{9}T_{12} - \frac{1}{6}(T_{15} + T_{16}),$$

$$\Delta T = \frac{8}{3}T_N - \frac{19}{2}T_0 + \frac{89}{36}T_2 + 2T_5 + \frac{49}{24}(T_3 + T_4) - \frac{11}{36}T_{12} - \frac{5}{12}(T_8 + T_{10}) - \frac{7}{24}(T_{15} + T_{16}).$$

e. $i=1$, $j=n_y$

We have

$$\partial_x T = -\frac{4}{3}T_S + T_0 + \frac{43}{72}T_1 - \frac{1}{48}(T_5 + T_6) - \frac{7}{72}T_9 - \frac{1}{12}(T_{11} + T_{13}) + \frac{1}{48}(T_{16} + T_{18}),$$

$$\partial_y T = \frac{5}{4}T_0 - \frac{5}{36}T_1 - \frac{3}{2}T_4 - \frac{1}{24}(T_5 + T_6 + T_{11} + T_{13}) + \frac{2}{9}T_9 + \frac{1}{6}(T_{16} + T_{18}),$$

$$\partial_z T = \frac{9}{8}(T_5 - T_6) - \frac{1}{6}(T_{11} - T_{13}) - \frac{1}{8}(T_{16} - T_{18}),$$

$$\Delta T = \frac{8}{3}T_S - \frac{19}{2}T_0 + \frac{89}{36}T_1 + 2T_4 + \frac{49}{24}(T_5 + T_6) - \frac{11}{36}T_9 - \frac{5}{12}(T_{11} + T_{13}) - \frac{7}{24}(T_{16} + T_{18}).$$

f. $i=1$, $j=1$

We have

$$\partial_x T = -\frac{4}{3}T_S + T_0 + \frac{43}{72}T_1 - \frac{1}{48}(T_5 + T_6) - \frac{7}{72}T_7 - \frac{1}{12}(T_{11} + T_{13}) + \frac{1}{48}(T_{15} + T_{17}),$$

$$\partial_y T = -\frac{5}{4}T_0 + \frac{5}{36}T_1 + \frac{3}{2}T_3 + \frac{1}{24}(T_5 + T_6 + T_{11} + T_{13}) - \frac{2}{9}T_7 - \frac{1}{6}(T_{15} + T_{17}),$$

$$\partial_z T = \frac{9}{8}(T_5 - T_6) - \frac{1}{6}(T_{11} - T_{13}) - \frac{1}{8}(T_{15} - T_{17}),$$

$$\Delta T = \frac{8}{3}T_S - \frac{19}{2}T_0 + \frac{89}{36}T_1 + 2T_3 + \frac{49}{24}(T_5 + T_6) - \frac{11}{36}T_7 - \frac{5}{12}(T_{11} + T_{13}) - \frac{7}{24}(T_{15} + T_{17}).$$

g. $i=1$, $k=n_z$

We have

$$\partial_x T = -\frac{4}{3}T_S + T_0 + \frac{43}{72}T_1 - \frac{1}{48}(T_3 + T_4) - \frac{7}{72}T_{13} - \frac{1}{12}(T_7 + T_9) + \frac{1}{48}(T_{17} + T_{18}),$$

$$\partial_y T = \frac{9}{8}(T_3 - T_4) - \frac{1}{6}(T_7 - T_9) - \frac{1}{8}(T_{17} - T_{18}),$$

$$\partial_z T = \frac{5}{4}T_0 - \frac{5}{36}T_1 - \frac{3}{2}T_6 - \frac{1}{24}(T_3 + T_4 + T_7 + T_9) + \frac{2}{9}T_{13} + \frac{1}{6}(T_{17} + T_{18}),$$

$$\Delta T = \frac{8}{3}T_S - \frac{19}{2}T_0 + \frac{89}{36}T_1 + 2T_6 + \frac{49}{24}(T_3 + T_4) - \frac{11}{36}T_{13} - \frac{5}{12}(T_7 + T_9) - \frac{7}{24}(T_{17} + T_{18}).$$

h. i=1, k=1

We have

$$\partial_x T = -\frac{4}{3}T_S + T_0 + \frac{43}{72}T_1 - \frac{1}{48}(T_3 + T_4) - \frac{7}{72}T_{11} - \frac{1}{12}(T_7 + T_9) + \frac{1}{48}(T_{15} + T_{16}),$$

$$\partial_y T = \frac{9}{8}(T_3 - T_4) - \frac{1}{6}(T_7 - T_9) - \frac{1}{8}(T_{15} - T_{16}),$$

$$\partial_z T = -\frac{5}{4}T_0 + \frac{5}{36}T_1 + \frac{3}{2}T_5 + \frac{1}{24}(T_3 + T_4 + T_7 + T_9) - \frac{2}{9}T_{11} - \frac{1}{6}(T_{15} + T_{16}),$$

$$\Delta T = \frac{8}{3}T_S - \frac{19}{2}T_0 + \frac{89}{36}T_1 + 2T_5 + \frac{49}{24}(T_3 + T_4) - \frac{11}{36}T_{11} - \frac{5}{12}(T_7 + T_9) - \frac{7}{24}(T_{15} + T_{16}).$$

i. j=n_y, k=n_z

We have

$$\partial_x T = \frac{3}{4}(T_1 - T_2) - \frac{1}{8}(T_9 - T_{10} + T_{13} - T_{14}),$$

$$\partial_y T = \frac{55}{64}T_0 - \frac{7}{64}(T_1 + T_2) - \frac{59}{64}T_4 - \frac{5}{64}T_6 + \frac{9}{64}(T_9 + T_{10} + T_{18}) - \frac{1}{32}(T_{13} + T_{14}),$$

$$\partial_z T = \frac{55}{64}T_0 - \frac{7}{64}(T_1 + T_2) - \frac{5}{64}T_4 - \frac{59}{64}T_6 + \frac{9}{64}(T_{13} + T_{14} + T_{18}) - \frac{1}{32}(T_9 + T_{10}),$$

$$\Delta T = -\frac{85}{16}T_0 + \frac{25}{16}(T_1 + T_2) + \frac{7}{4}(T_4 + T_6) - \frac{9}{32}(T_9 + T_{10} + T_{13} + T_{14}) - \frac{3}{16}(T_{18}).$$

j. j=n_y, k=1

We have

$$\partial_x T = \frac{3}{4}(T_1 - T_2) - \frac{1}{8}(T_9 - T_{10} + T_{11} - T_{12}),$$

$$\partial_y T = \frac{55}{64}T_0 - \frac{7}{64}(T_1 + T_2) - \frac{59}{64}T_4 - \frac{5}{64}T_5 + \frac{9}{64}(T_9 + T_{10} + T_{16}) - \frac{1}{32}(T_{11} + T_{12}),$$

$$\partial_z T = -\frac{55}{64}T_0 + \frac{7}{64}(T_1 + T_2) + \frac{5}{64}T_4 + \frac{59}{64}T_5 - \frac{9}{64}(T_{11} + T_{12} + T_{16}) + \frac{1}{32}(T_9 + T_{10}),$$

$$\Delta T = -\frac{85}{16}T_0 + \frac{25}{16}(T_1 + T_2) + \frac{7}{4}(T_4 + T_5) - \frac{9}{32}(T_9 + T_{10} + T_{11} + T_{12}) - \frac{3}{16}(T_{16}).$$

k. j=1, k=n_z

We have

$$\partial_x T = \frac{3}{4}(T_1 - T_2) - \frac{1}{8}(T_7 - T_8 + T_{13} - T_{14}),$$

$$\partial_y T = -\frac{55}{64}T_0 + \frac{7}{64}(T_1 + T_2) + \frac{59}{64}T_3 + \frac{5}{64}T_6 - \frac{9}{64}(T_7 + T_8 + T_{17}) + \frac{1}{32}(T_{13} + T_{14}),$$

$$\partial_z T = \frac{55}{64}T_0 - \frac{7}{64}(T_1 + T_2) - \frac{5}{64}T_3 - \frac{59}{64}T_6 + \frac{9}{64}(T_{13} + T_{14} + T_{17}) - \frac{1}{32}(T_7 + T_8),$$

$$\Delta T = -\frac{85}{16}T_0 + \frac{25}{16}(T_1 + T_2) + \frac{7}{4}(T_2 + T_6) - \frac{9}{32}(T_7 + T_8 + T_{13} + T_{14}) - \frac{3}{16}(T_{17}).$$

l. j=1, k=1

We have

$$\partial_x T = \frac{3}{4}(T_1 - T_2) - \frac{1}{8}(T_7 - T_8 + T_{11} - T_{12}),$$

$$\partial_y T = -\frac{55}{64}T_0 + \frac{7}{64}(T_1 + T_2) + \frac{59}{64}T_3 + \frac{5}{64}T_5 - \frac{9}{64}(T_7 + T_8 + T_{15}) - \frac{1}{32}(T_{11} + T_{12}),$$

$$\partial_z T = -\frac{55}{64}T_0 + \frac{7}{64}(T_1 + T_2) + \frac{5}{64}T_3 + \frac{59}{64}T_5 - \frac{9}{64}(T_{11} + T_{12} + T_{15}) + \frac{1}{32}(T_7 + T_8),$$

$$\Delta T = -\frac{85}{16}T_0 + \frac{25}{16}(T_1 + T_2) + \frac{7}{4}(T_3 + T_5) - \frac{9}{32}(T_9 + T_{10} + T_{11} + T_{12}) - \frac{3}{16}(T_{15}).$$

4. Corners

a. i=n_x, j=n_y, k=n_z

We have

$$\partial_x T = \frac{4}{3}T_N - \frac{89}{96}T_0 - \frac{19}{36}T_2 - \frac{1}{32}(T_4 + T_6) + \frac{7}{72}(T_{10} + T_{14}) - \frac{1}{96}T_{18},$$

$$\partial_y T = \frac{121}{96}T_0 - \frac{7}{36}T_2 - \frac{43}{32}T_4 - \frac{3}{32}T_6 + \frac{2}{9}T_{10} - \frac{1}{36}T_{14} + \frac{17}{96}T_{18},$$

$$\partial_z T = \frac{121}{96}T_0 - \frac{7}{36}T_2 - \frac{3}{32}T_4 - \frac{43}{32}T_6 - \frac{1}{36}T_{10} + \frac{2}{9}T_{14} + \frac{17}{96}T_{18},$$

$$\Delta T = \frac{8}{3}T_N - \frac{355}{48}T_0 + \frac{37}{18}T_2 + \frac{29}{16}(T_4 + T_6) - \frac{13}{36}(T_{10} + T_{14}) - \frac{11}{48}T_{18}.$$

b. i=n_x, j=n_y, k=1

We have

$$\partial_x T = \frac{4}{3}T_N - \frac{89}{96}T_0 - \frac{19}{36}T_2 - \frac{1}{32}(T_4 + T_5) + \frac{7}{72}(T_{10} + T_{12}) - \frac{1}{96}T_{16},$$

$$\partial_y T = \frac{121}{96}T_0 - \frac{7}{36}T_2 - \frac{43}{32}T_4 - \frac{3}{32}T_5 + \frac{2}{9}T_{10} - \frac{1}{36}T_{12} + \frac{17}{96}T_{16},$$

$$\partial_z T = -\frac{121}{96}T_0 + \frac{7}{36}T_2 + \frac{3}{32}T_4 + \frac{43}{32}T_5 + \frac{1}{36}T_{10} - \frac{2}{9}T_{12} - \frac{17}{96}T_{16},$$

$$\Delta T = \frac{8}{3}T_N - \frac{355}{48}T_0 + \frac{37}{18}T_2 + \frac{29}{16}(T_4 + T_5) - \frac{13}{36}(T_{10} + T_{12}) - \frac{11}{48}T_{16}.$$

c. i=n_x, j=1, k=n_z

We have

$$\partial_x T = \frac{4}{3}T_N - \frac{89}{96}T_0 - \frac{19}{36}T_2 - \frac{1}{32}(T_3 + T_6) + \frac{7}{72}(T_8 + T_{14}) - \frac{1}{96}T_{17},$$

$$\partial_y T = -\frac{121}{96}T_0 + \frac{7}{36}T_2 + \frac{43}{32}T_3 + \frac{3}{32}T_6 - \frac{2}{9}T_8 + \frac{1}{36}T_{14} - \frac{17}{96}T_{17},$$

$$\partial_z T = \frac{121}{96}T_0 - \frac{7}{36}T_2 - \frac{3}{32}T_3 - \frac{43}{32}T_6 - \frac{1}{36}T_8 + \frac{2}{9}T_{14} + \frac{17}{96}T_{17},$$

$$\Delta T = \frac{8}{3}T_N - \frac{355}{48}T_0 + \frac{37}{18}T_2 + \frac{29}{16}(T_3 + T_6) - \frac{13}{36}(T_8 + T_{14}) - \frac{11}{48}T_{17}.$$

d. i=n_x, j=1, k=1

We have

$$\partial_x T = \frac{4}{3}T_N - \frac{89}{96}T_0 - \frac{19}{36}T_2 - \frac{1}{32}(T_3 + T_5) + \frac{7}{72}(T_8 + T_{12}) - \frac{1}{96}T_{15},$$

$$\partial_y T = -\frac{121}{96}T_0 + \frac{7}{36}T_2 + \frac{43}{32}T_3 + \frac{3}{32}T_5 - \frac{2}{9}T_8 + \frac{1}{36}T_{12} - \frac{17}{96}T_{15},$$

$$\partial_z T = -\frac{121}{96}T_0 + \frac{7}{36}T_2 + \frac{3}{32}T_3 + \frac{43}{32}T_5 + \frac{1}{36}T_8 - \frac{2}{9}T_{12} - \frac{17}{96}T_{15},$$

$$\Delta T = \frac{8}{3}T_N - \frac{355}{48}T_0 + \frac{37}{18}T_2 + \frac{29}{16}(T_3 + T_5) - \frac{13}{36}(T_8 + T_{12}) - \frac{11}{48}T_{15}.$$

e. $i=1$, $j=n_y$, $k=n_z$

We have

$$\partial_x T = -\frac{4}{3}T_S + \frac{89}{96}T_0 + \frac{19}{36}T_1 + \frac{1}{32}(T_4 + T_6) - \frac{7}{72}(T_9 + T_{13}) + \frac{1}{96}T_{18},$$

$$\partial_y T = \frac{121}{96}T_0 - \frac{7}{36}T_1 - \frac{43}{32}T_4 - \frac{3}{32}T_6 + \frac{2}{9}T_9 - \frac{1}{36}T_{13} + \frac{17}{96}T_{18},$$

$$\partial_z T = \frac{121}{96}T_0 - \frac{7}{36}T_1 - \frac{3}{32}T_4 - \frac{43}{32}T_6 - \frac{1}{36}T_9 + \frac{2}{9}T_{13} + \frac{17}{96}T_{18},$$

$$\Delta T = \frac{8}{3}T_S - \frac{355}{48}T_0 + \frac{37}{18}T_1 + \frac{29}{16}(T_4 + T_6) - \frac{13}{36}(T_9 + T_{13}) - \frac{11}{48}T_{18}.$$

f. $i=1$, $j=n_y$, $k=1$

We have

$$\partial_x T = -\frac{4}{3}T_S + \frac{89}{96}T_0 + \frac{19}{36}T_1 - \frac{1}{32}(T_4 + T_5) - \frac{7}{72}(T_9 + T_{11}) + \frac{1}{96}T_{16},$$

$$\partial_y T = \frac{121}{96}T_0 - \frac{7}{36}T_1 - \frac{43}{32}T_4 - \frac{3}{32}T_5 + \frac{2}{9}T_9 - \frac{1}{36}T_{11} + \frac{17}{96}T_{16},$$

$$\partial_z T = -\frac{121}{96}T_0 + \frac{7}{36}T_1 + \frac{3}{32}T_4 + \frac{43}{32}T_5 + \frac{1}{36}T_9 - \frac{2}{9}T_{11} - \frac{17}{96}T_{16},$$

$$\Delta T = \frac{8}{3}T_N - \frac{355}{48}T_0 + \frac{37}{18}T_1 + \frac{29}{16}(T_4 + T_5) - \frac{13}{36}(T_9 + T_{11}) - \frac{11}{48}T_{16}.$$

g. $i=1$, $j=1$, $k=n_z$

We have

$$\partial_x T = -\frac{4}{3}T_S + \frac{89}{96}T_0 + \frac{19}{36}T_1 + \frac{1}{32}(T_3 + T_6) - \frac{7}{72}(T_7 + T_{13}) + \frac{1}{96}T_{17},$$

$$\partial_y T = -\frac{121}{96}T_0 + \frac{7}{36}T_1 + \frac{43}{32}T_3 + \frac{3}{32}T_6 - \frac{2}{9}T_7 + \frac{1}{36}T_{13} - \frac{17}{96}T_{17},$$

$$\partial_z T = \frac{121}{96}T_0 - \frac{7}{36}T_1 - \frac{3}{32}T_3 - \frac{43}{32}T_6 - \frac{1}{36}T_7 + \frac{2}{9}T_{13} + \frac{17}{96}T_{17},$$

$$\Delta T = \frac{8}{3}T_N - \frac{355}{48}T_0 + \frac{37}{18}T_1 + \frac{29}{16}(T_3 + T_6) - \frac{13}{36}(T_7 + T_{13}) - \frac{11}{48}T_{17}.$$

h. $i=1$, $j=1$, $k=1$

We have

$$\partial_x T = -\frac{4}{3}T_S + \frac{89}{96}T_0 + \frac{19}{36}T_1 + \frac{1}{32}(T_3 + T_5) - \frac{7}{72}(T_7 + T_{11}) + \frac{1}{96}T_{15},$$

$$\partial_y T = -\frac{121}{96}T_0 + \frac{7}{36}T_1 + \frac{43}{32}T_3 + \frac{3}{32}T_5 - \frac{2}{9}T_7 + \frac{1}{36}T_{11} - \frac{17}{96}T_{15},$$

$$\partial_z T = -\frac{121}{96}T_0 + \frac{7}{36}T_1 + \frac{3}{32}T_3 + \frac{43}{32}T_5 + \frac{1}{36}T_7 - \frac{2}{9}T_{11} - \frac{17}{96}T_{15},$$

$$\Delta T = \frac{8}{3}T_N - \frac{355}{48}T_0 + \frac{37}{18}T_1 + \frac{29}{16}(T_3 + T_5) - \frac{13}{36}(T_7 + T_{11}) - \frac{11}{48}T_{15}.$$

[1] J. S. Turner, Annu. Rev. Fluid Mech. **6**, 37 (1974).
[2] S. Ostrach, PCH, PhysicoChem. Hydrodyn. **1**, 233 (1980).
[3] J. S. Turner, *Buoyancy Effects in Fluids*, Cambridge Monographs on Mechanics and Applied Mathematics (Cambridge University Press, Cambridge, 1973).
[4] J. S. Turner, Annu. Rev. Fluid Mech. **17**, 11 (1985).
[5] I. Sezai and A. A. Mohamad, Phys. Fluids **12**, 2210 (2000).
[6] Y. Kamotani, L. W. Wang, S. Ostrach, and H. D. Jiang, Int. J. Heat Mass Transfer **28**, 165 (1985).
[7] J. Lee, M. T. Hyun, and K. W. Kim, Int. J. Heat Mass Transfer **31**, 1969 (1988).
[8] J. A. Weaver and R. Viskanta, J. Heat Transfer **113**, 141 (1991).
[9] H. D. Jiang, S. Ostrach, and Y. Kamotani, J. Heat Transfer **113**, 135 (1991).
[10] H. Han and T. H. Kuehn, Int. J. Heat Mass Transfer **34**, 449 (1991).
[11] J. W. Lee and J. M. Hyun, Int. J. Heat Mass Transfer **33**, 1619 (1990).
[12] J. W. Lee and J. M. Hyun, Int. J. Heat Mass Transfer **34**, 2409 (1991).
[13] H. Han and T. H. Kuehn, Int. J. Heat Mass Transfer **34**, 461 (1991).
[14] C. Béghein, F. Haghighat, and F. Allard, Int. J. Heat Mass Transfer **35**, 833 (1992).
[15] W. Shyy and M.-H. Chen, Phys. Fluids A **3**, 2592 (1991).
[16] D. Gobin and R. Bennacer, Phys. Fluids **6**, 59 (1994).
[17] R. Bennacer and D. Gobin, Int. J. Heat Mass Transfer **39**, 2671 (1996).
[18] D. Gobin and R. Bennacer, Int. J. Heat Mass Transfer **39**, 2683 (1996).
[19] K. Ghorayeb and A. Mojtabi, Phys. Fluids **9**, 2339 (1997).
[20] S. Xin, P. Le Quéré, and L. S. Tuckerman, Phys. Fluids **10**, 850 (1998).
[21] A. Bergeon, K. Ghorayeb, and A. Mojtabi, Phys. Fluids **11**, 549 (1999).
[22] K. Ghorayeb, H. Khallouf, and A. Mojtabi, Int. J. Heat Mass Transfer **42**, 629 (1999).
[23] A. Bergeon and E. Knobloch, Phys. Fluids **14**, 3233 (2002).
[24] J. W. Lee and J. M. Hyun, Int. J. Heat Mass Transfer **33**, 1605 (1990).
[25] T. L. Bergman and M. T. Hyun, Int. J. Heat Mass Transfer **39**, 2883 (1996).
[26] X. He and L.-S. Luo, Phys. Rev. E **55**, R6333 (1997).
[27] X. He and L.-S. Luo, Phys. Rev. E **56**, 6811 (1997).
[28] X. Shan and X. He, Phys. Rev. Lett. **80**, 65 (1998).
[29] X. Shan, X. Yuan, and H. Chen, J. Fluid Mech. **550**, 413 (2006).
[30] A. Gunstensen and D. Rothman, J. Geophys. Res. **98**, 6431 (1993).
[31] N. S. Martys and H. Chen, Phys. Rev. E **53**, 743 (1996).
[32] C. Pan, L.-S. Luo, and C. Miller, Comput. Fluids **35**, 898 (2006).
[33] X. Shan and G. D. Doolen, J. Stat. Phys. **81**, 379 (1995).
[34] E. Orlandini, M. R. Swift, and J. M. Yeomans, Europhys. Lett. **32**, 463 (1995).
[35] L.-S. Luo and S. S. Girimaji, Phys. Rev. E **67**, 036302 (2003).
[36] P. Asinari, Phys. Fluids **17**, 067102 (2005).
[37] X. Shan and H. Chen, Phys. Rev. E **47**, 1815 (1993).
[38] M. R. Swift, E. Orlandini, W. R. Osborn, and J. M. Yeomans, Phys. Rev. E **54**, 5041 (1996).
[39] L.-S. Luo, Phys. Rev. Lett. **81**, 1618 (1998).
[40] A. J. C. Ladd, J. Fluid Mech. **271**, 285 (1994).
[41] D. Qi, J. Fluid Mech. **385**, 43 (1999).
[42] P. Lallemand and L.-S. Luo, Phys. Rev. E **68**, 036706 (2003).
[43] P. Lallemand and L.-S. Luo, Int. J. Mod. Phys. B **17**, 41 (2003).
[44] R. Y. Zhang and H. D. Chen, Phys. Rev. E **67**, 066711 (2003).
[45] F. Verhaeghe, S. Arnout, B. Blanpain, and P. Wollants, Phys. Rev. E **73**, 036316 (2006).
[46] F. P. Incropera and D. P. DeWitt, *Fundamentals of Heat and Mass Transfer*, 5th ed. (Wiley, New York, 2002).
[47] R. B. Bird, W. E. Stewart, and E. N. Lightfoot, *Transport Phenomena*, 2nd ed. (Wiley, New York, 2001).
[48] L.-S. Luo and S. S. Girimaji, Phys. Rev. E **66**, 035301(R) (2002).
[49] L. Sirovich, Phys. Fluids **5**, 908 (1962).
[50] I. Ginzburg and D. d'Humières, Phys. Rev. E **68**, 066614 (2003).
[51] G. De Vahl Davis, Int. J. Numer. Methods Fluids **3**, 249 (1983).
[52] T. Fusegi, J. M. Hyun, K. Kuwahara, and B. Farouk, Int. J. Heat Mass Transfer **34**, 1543 (1991).
[53] Y. Peng, C. Shu, and Y. T. Chew, J. Comput. Phys. **193**, 260 (2003).